water

Article

Impact of the Boreholes on the Surrounding Ground

Sudip Shakya [1], Koki Nakao [1], Shuichi Kuwahara [2] and Shinya Inazumi [3,*]

[1] Graduate School of Engineering and Science, Shibaura Institute of Technology, Tokyo 135-8548, Japan
[2] Japan Association for Pulling-Out Existing Piles, Tokyo 152-0004, Japan
[3] College of Engineering, Shibaura Institute of Technology, Tokyo 135-8548, Japan
* Correspondence: inazumi@shibaura-it.ac.jp; Tel.: +81-3-5859-8360

Abstract: The infrastructures that were constructed decades ago do not meet the present structural benchmark, and they need to be demolished. In order to reclaim these lands, the existing pile foundations must be removed; otherwise, the land will lose its value. Since the piles are pulled out, vacant spaces are created in the ground. This causes the surrounding ground to experience settlement, jeopardizing its stability. The degree of influence depends upon the number of boreholes, the saturated condition of the ground, the time period of the vacant condition, the presence of loading, etc. It is important to understand the scope of the probable settlement under various situations. This study focused on determining the amount of displacement and its range for three different saturated soil types under loaded and unloaded conditions using the finite element method (FEM) analysis. It was observed that stiff ground underwent maximum deformation, while soft ground experienced the maximum influence from external factors. Moreover, the presence of loading not only increased the displacement amount and range, but it also caused a change in the location of the maximum displacement.

Keywords: land reclaim; pile removal; finite element method; ground settlement; loading condition

check for updates

Citation: Shakya, S.; Nakao, K.; Kuwahara, S.; Inazumi, S. Impact of the Boreholes on the Surrounding Ground. *Water* **2023**, *15*, 188. https://doi.org/10.3390/w15010188

Academic Editors: Panpan Guo, Yixian Wang, Hang Lin and Yanlin Zhao

Received: 15 October 2022
Revised: 5 November 2022
Accepted: 24 November 2022
Published: 2 January 2023

1. Introduction

The industrialization period brought rapid economic growth, with lots of infrastructures being constructed all over the world. Those infrastructures have now become obsolete due to the constant updating of building standards, and many have surpassed their lifespan [1]. Thus, they need to be demolished in the near future [2,3]. The chances of these infrastructures being supported by pile foundations are high; thus, the removal of the existing piles is compulsory if the land is to be resold [4–7]. The pile removal process should be carried out carefully so that errors, such as crushing the piles or leaving portions of them in the ground, can be avoided [5–10]. The pile tip chucking method [11] is a recently developed pile pulling method in which the entire pile is wrapped by chucking and efficiently pulled upward, even in difficult cases of mid-breaks or defective joints. Meanwhile, if the boreholes that remain after the existing piles are pulled out are left hollow, the collapse and deformation of the surrounding ground may occur [12]. This causes the concern of ground instability in the vicinity of the boreholes even during the borehole excavation operation. The loading exerted by heavy machinery and the vibrations produced during the operation contribute to the deformation of the surrounding ground. Moreover, the material deposited in the surrounding ground also contributes to the ground deformation. If these boreholes are left vacant, the ground may undergo further deformation. However, filling the excavation holes with treated soil, such as sand, fluidized soil, cement milk, or the equivalent, after removing the existing piles will help reduce the adverse effects [13–15]. Unfortunately, despite these measures, the chances of ground deformation cannot be completely prevented because the treated soil will require 7 to 28 days to fully gain strength, and if there are other important infrastructures nearby, the deformation of the ground may then have adverse effects on their structural integrity. Therefore, it is very important to have clear knowledge of the deformation behavior of the ground.

Wheeler et al. [16], Wheeler [17], Alonso et al. [18], and Fredlund and Morgenstern [19,20] showed that the degree of saturation has a significant influence on the stress-strain behavior of unsaturated soil and that the soil deformation undergoes a continuous elasto-plastic change process. In this study, the authors attempted to quantify the amount of ground deformation for different degrees of saturation using an elasto-plastic model, i.e., the modified Cam-Clay model, with and without the influence of loading, by a finite element method analysis [21–24] so that the adverse effect of ground settlement and instability during pile removal could be tackled.

2. Analysis

2.1. Model and Method

Figure 1a,b shows the analytical models, 50 × 50 × 25 m, for the single and double boreholes. Both models are composed of two different layers showing the typical ground that needs pile foundation for constructing infrastructures. The upper 18 m is a ground layer composed of clay, and the lower 7 m is a bearing layer composed of sand. The properties of the bearing layer remain constant in all the simulations. Meanwhile, the ground layer is assumed to comprise three different clays with different parameters for each simulation. The boreholes are 2 m in diameter, 20 m in depth, and 4 m apart from each other.

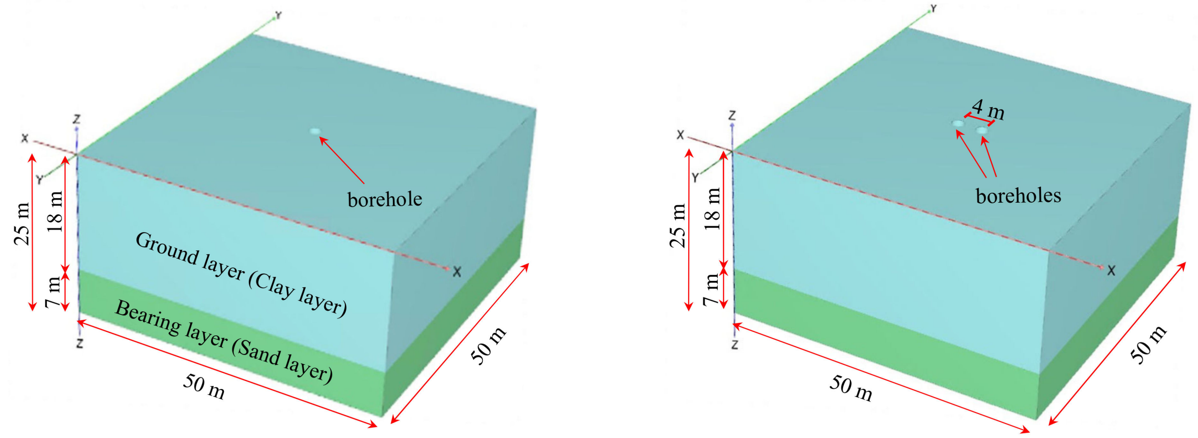

(**a**) Ground model for single borehole. (**b**) Ground model for double boreholes.

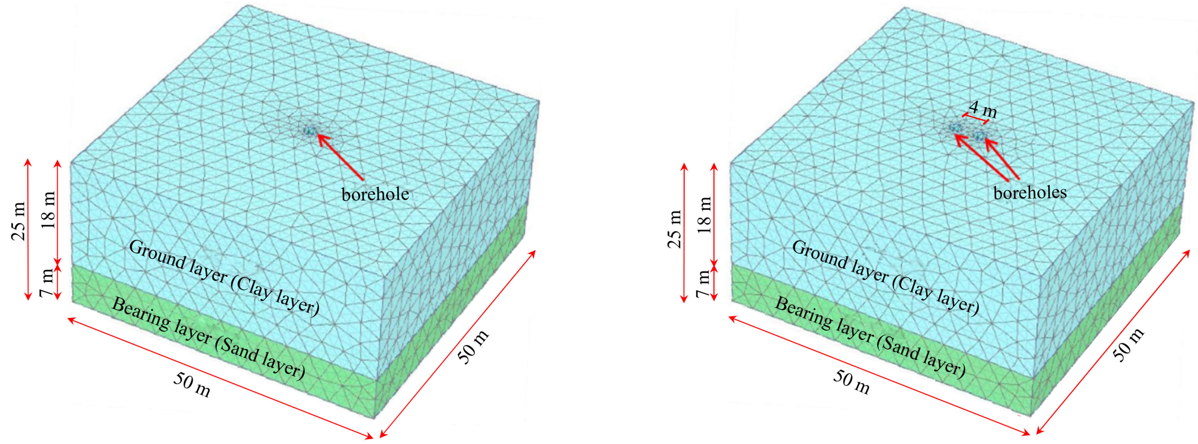

(**c**) Meshing for single borehole. (**d**) Meshing for double boreholes.

Figure 1. Analytical ground models for single and double boreholes.

Figure 1c,d shows the meshing of the analytical models. Each analytical model was subjected to a finite element method (FEM) analysis using PLAXIS 3D software after the model was divided into a certain number of triangular meshes during the simulations. The mesh size was set to be of smaller size and more concentrated around the boreholes in comparison to other areas so that the simulation accuracy could be increased. The literature review revealed that the soil deformation is the continuous elasto-plastic change process, and the soil showed the complex behavior as a three-dimensional analysis object. Thus, for clay, the elastoplastic model [25] was selected because of its elasticity and plasticity properties. An advanced geotechnical analysis that uses the finite element method is often based on an isotropic elastoplastic model, e.g., the modified Cam-Clay model for clay [26,27]. The modified Cam-Clay model [28–30] is an elasto-plastic strain-hardening model that is based on the critical state theory. Additionally, this model produces the more accurate shear behavior of soil, and it requires only three main parameters, i.e., compression index (λ), swelling index (κ), and the critical stress ration (M), which can be easily determined. Thus, the modified Cam-Clay model was applied to the ground layer, whereas the Mohr-Coulomb model was applied to the bearing layer and the filler material. The drainage condition was set as top-bottom drainage and left-right drainage to increase the accuracy of the simulation.

2.2. Parameters

Table 1 shows the input parameters for the clays of different hardness, while Table 2 shows the input parameters for the filler material and bearing layer. The values for the irrelevant parameters in this simulation are not given. The values for the filler material and bearing layer parameters in Table 2 were taken from Kawahara et al. [11]. The modified Cam-Clay model was applied to the ground layer; Xu et al. [31] reported the applicability of this model to consolidated soil and over-consolidated soft clays. In this study, all three clays were considered to have an over-consolidation ratio (OCR) of 1, representing a normal consolidation state. Ikegami et al. [32] and Murakami et al. [33] analyzed the model using actual data measured in the field for the parameter values or set the values by referring to the measured N-values. In this study, however, the values for the parameters in the simulations were derived from the relations of one parameter with another. Kawamura et al. [34] suggested relationships for calculating the values of the compaction index and swelling index from the natural water contents for the simulations. Meanwhile, the methods used to determine other parameters are explained below.

Table 1. Input parameters for the clays of different hardness.

w_n	N-Value	γ_{unsat} (kN/m^3)	γ_{sat} (kN/m^3)	ν	λ	κ	M	K_0	OCR	e_0	k_p (m/d)	Ground Classification
30%	8.88	16	17	0.277	0.107	0.012	1.555	0.383	1	0.817	2.23×10^{-2}	Stiff
40%	6.99	15	16	0.276	0.164	0.018	1.562	0.380	1	1.089	4.34×10^{-3}	Medium
80%	2.68	13	14	0.274	0.389	0.04	1.569	0.378	1	2.177	8.47×10^{5}	Soft

Table 2. Input parameters for the filler material and bearing layer.

Material	γ_{unsat} (kN/m^3)	γ_{sat} (kN/m^3)	q_u (kN/m^3)	E (kN/m^3)	ν (-)	Φ (°)	C (kN/m^2)	k_p (m/d)	N-Value
Filler material	14	15	100	136,223	0.48	26	50	8.64×10^{-5}	-
Bearing layer	20	21	-	1.4×10^{5}	0.3	-	0	0.864	50

Uniaxial compressive strength (q_u): The uniaxial compressive strength of clay with a certain water content was calculated with Equation (1), while the N-value of the clay was calculated with Equation (2):

$$q_u = 255.5e^{-0.024w_n} \tag{1}$$

$$q_u = 14N \tag{2}$$

where q_u is the uniaxial compressive strength, N is the N-value of the clay, w_n is the natural water content, and e is the base of the natural logarithm.

Unit weight volume (γ): The consistency of each clay type was confirmed by the calculated value for N and was categorized as stiff, medium, or soft for 30, 40, or 80% water contents, respectively. After that, the unit weight of each clay was determined based on its consistency from the Road Earthworks-Embankment Guidelines 2022 [35].

Compression index (C_c): The compression index was calculated from the natural water content (w_n), as shown in Equation (3), while the compression index (λ) used in the modified Cam-Clay model was calculated with Equation (4):

$$C_c = 0.013\,(w_n - 11) \tag{3}$$

$$\lambda = 0.434 C_c \tag{4}$$

where C_c is the compression index, and λ is the compression index used in the modified Cam-Clay model.

Swelling index (C_s): The swelling index was calculated from the natural water content (w_n), shown in Equation (5), while the swelling index (κ) used in the modified Cam-Clay model was calculated with Equation (6).

$$C_s = 0.0013\,(w_n - 8.8) \tag{5}$$

$$\kappa = 0.434 C_s \tag{6}$$

where C_s is the swelling index, and κ is the swelling index used in the modified Cam-Clay model.

Critical stress ratio (M): The irreversible ratio (Λ) was calculated from the compressive index (λ) and the swelling index (κ), shown in Equation (7), while the critical stress ratio (M) was calculated from the irreversible ratio (Λ), shown in Equation (8).

$$\Lambda = 1 - \frac{\kappa}{\lambda} \tag{7}$$

$$M = \Lambda * 1.75 \tag{8}$$

where Λ is the irreversible ratio and M is the critical stress ratio.

Coefficient of earth pressure at rest (K_0): Using Equation (9), $\sin \Phi$ was calculated from the critical stress ratio, and the coefficient of static earth pressure was calculated from $\sin \Phi$, as shown in Equation (10):

$$M = \frac{6 \sin \Phi}{3 - \sin \Phi} \tag{9}$$

$$K_0 = 1 - \sin \Phi \tag{10}$$

where Φ is the internal friction angle, and K_0 is the coefficient of static earth pressure.

Poisson's ratio (ν): Poisson's ratio was calculated with Equation (11):

$$\nu = \frac{K_0}{1 - K_0} \tag{11}$$

where ν is Poisson's ratio, which is calculated from the static earth pressure coefficient.

Void ratio (e_0): As shown in Equation (12), the void ratio was calculated from the compression index:

$$C_c = 0.478\,(e_0 - 0.3) \tag{12}$$

where e_0 is the void ratio.

Hydraulic conductivity (k_p): The hydraulic conductivity was calculated as shown in Equation (13):

$$k_p = 6322.7 {w_n}^{-5.68} \tag{13}$$

where k_p is the hydraulic conductivity, which is calculated from the natural water content.

3. Results and Discussion

3.1. Influence of Boreholes on Surrounding Ground under Unloaded Condition

3.1.1. In Case of Single Boreholes Left Vacant

Figure 2 shows the top views of the displacement contour for single boreholes left vacant. It is seen that the surrounding area of influence has a circular shape. The maximum displacement vectors for single boreholes without loading for stiff, medium, and soft grounds were observed at (25, 26, 0), (25, 26, 0), and (25.903, 25.429, −0.710), respectively. Figure 3 shows a comparison of the rates of change in the maximum displacement vectors of single boreholes. Soft ground underwent the least displacement, whereas stiff and medium grounds underwent approximately equal displacement at the end of the simulation. The initial increment in displacement had a higher value for stiffer ground and a lower value for the stabilization time for the softer ground. The total displacement values at the end of the 29-day simulation for stiff, medium, and soft grounds were 35, 34.3, and 13.6 mm, respectively. Additionally, the time periods required for the stabilization were 8, 15, and 1.25 days, respectively. The reason for the stiff clay having the maximum deformation might lie in the optimum water content of the soil. It is established fact that the maximum soil deformation occurs at the optimum water content under loading, and as confirmed from the result, the chances of the stiff soil having a 30% natural water content, which would be closer to the optimum water content than 40% and 80%, is high.

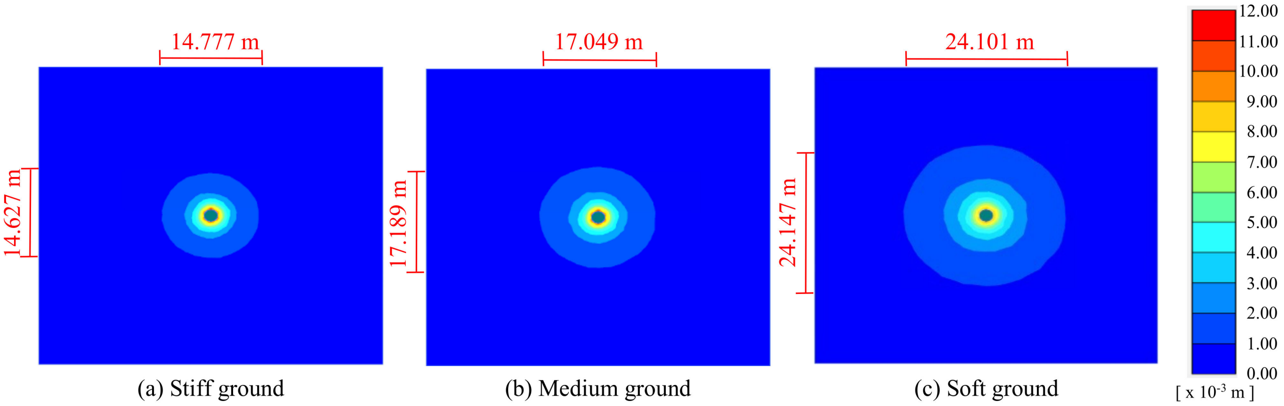

(a) Stiff ground (b) Medium ground (c) Soft ground

Figure 2. Top views of displacement contour for single boreholes left vacant.

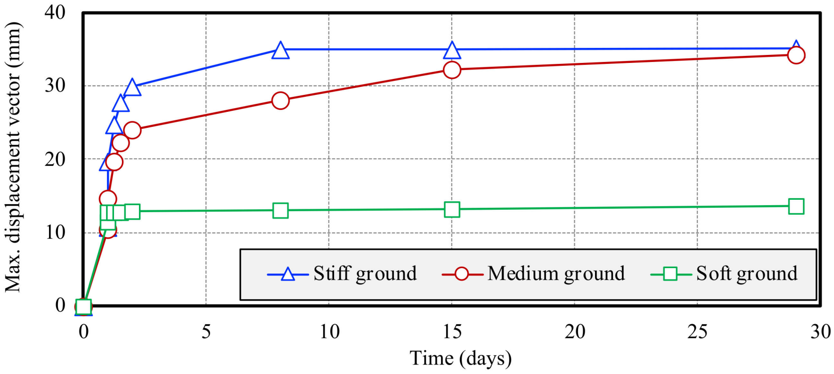

Figure 3. Rates of change in maximum displacement vectors for single boreholes left vacant.

3.1.2. In Case of Double Boreholes Left Vacant

Figure 4 shows the top views of the displacement contour for double boreholes left vacant. The influential area is elliptical in shape, with the highest degree of influence around the vicinity of the borehole. The maximum displacement vector was observed at the coordinates of (26.866, 25.5, 0), (26.866, 25.5, 0), and (23.966, 25.259, −0.428) for stiff, medium, and soft grounds, respectively. Figure 5 shows a comparison of the rates of change in the maximum displacement vectors of double boreholes. Figures 6 and 7 show a comparison of the total stress and pore water pressure of the double boreholes, respectively. The displacement and stabilization patterns, when compared to those of the single boreholes left vacant, were found to be similar, except for medium ground, which continued to deform until the end of the simulation period, and the final displacement value became greater than that of the stiff ground. Considering the result for the single borehole deformation, it can be concluded that the 40% water content also might not be farther from the optimum water content than 30%, but the presence of the extra borehole might have triggered an additional factor in deformation. The total displacement values for stiff, medium, and soft grounds were observed to be 46.4, 49, and 17.8 mm, respectively. The displacement value was higher compared to the single borehole, suggesting that the increase in the number of boreholes contributed to a higher deformation.

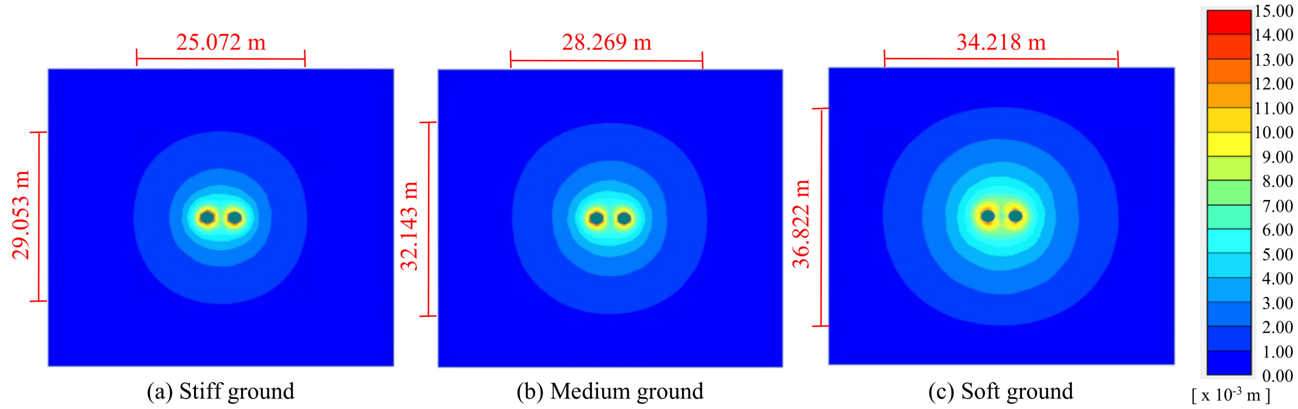

(a) Stiff ground (b) Medium ground (c) Soft ground

Figure 4. Top views of displacement contour for double boreholes left vacant.

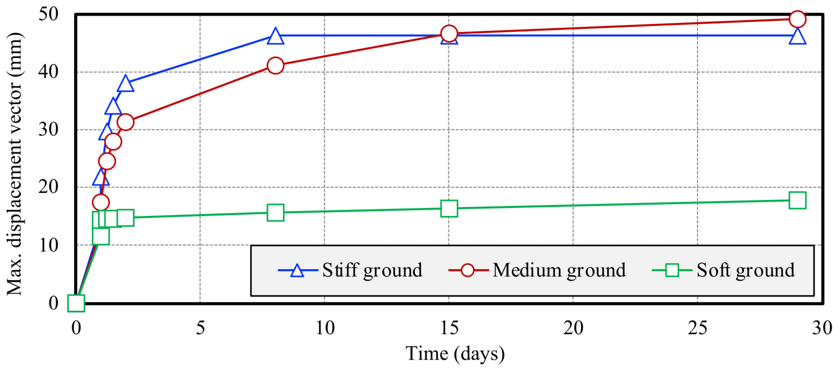

Figure 5. Rates of change in maximum displacement vectors for double boreholes left vacant.

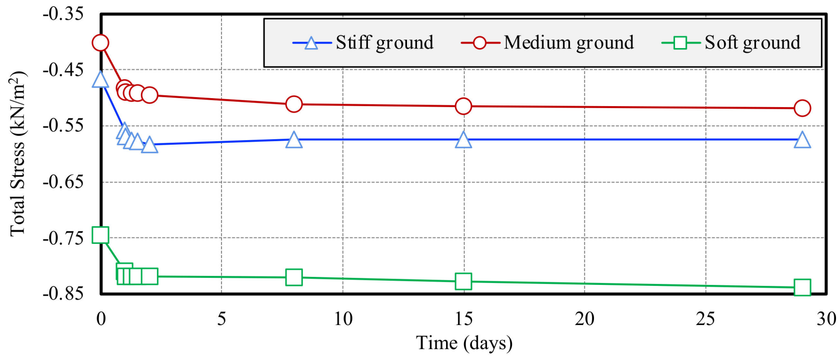

Figure 6. Rates of change in total stress for double boreholes left vacant.

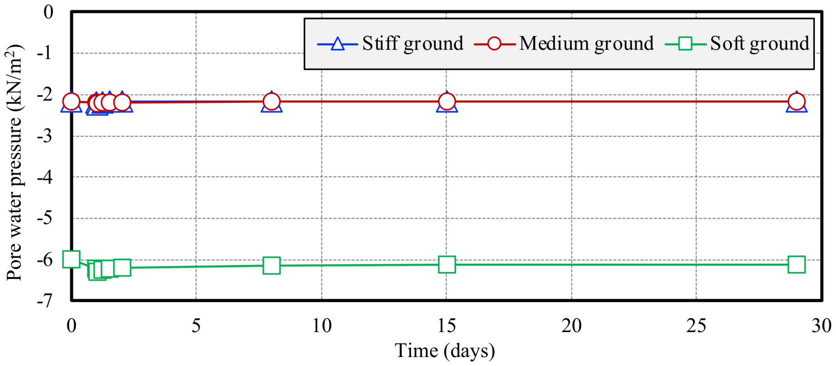

Figure 7. Rates of change in pore water pressure for double boreholes left vacant.

Soft ground had lower values for the initial total stress and pore water pressure compared to stiff and medium grounds. All the ground types experienced a reduction in value during the simulation. The total stress amounts for stiff and medium grounds started stabilizing after an 8-day period, but they continued to decrease for soft ground. Meanwhile, the pore water pressure initially decreased rapidly, but it continued to increase after 1 day until it reached a stabilized value. This recovery period was the shortest for stiff ground and the longest for soft ground.

3.1.3. Comparison of Cases of Vacant and Filled Double Boreholes

From the analysis of the vacant and filled conditions, it was seen that the rate of the surrounding ground deformation immediately after the borehole excavation was rapid and of the maximum value. In this study, a comparison was made of the amount of sinking of the surrounding ground and the pore water pressure for vacant and filled conditions. Figure 8 shows a comparison of the frontal cross sectional, i.e., the XZ plane total stress contour, in the cases of double boreholes left vacant and after being filled with the filler material. After the boreholes were filled, the stress concentrating around the boreholes decreased, and the stress at the bottom of the boreholes dissipated, resulting in an increase in stress.

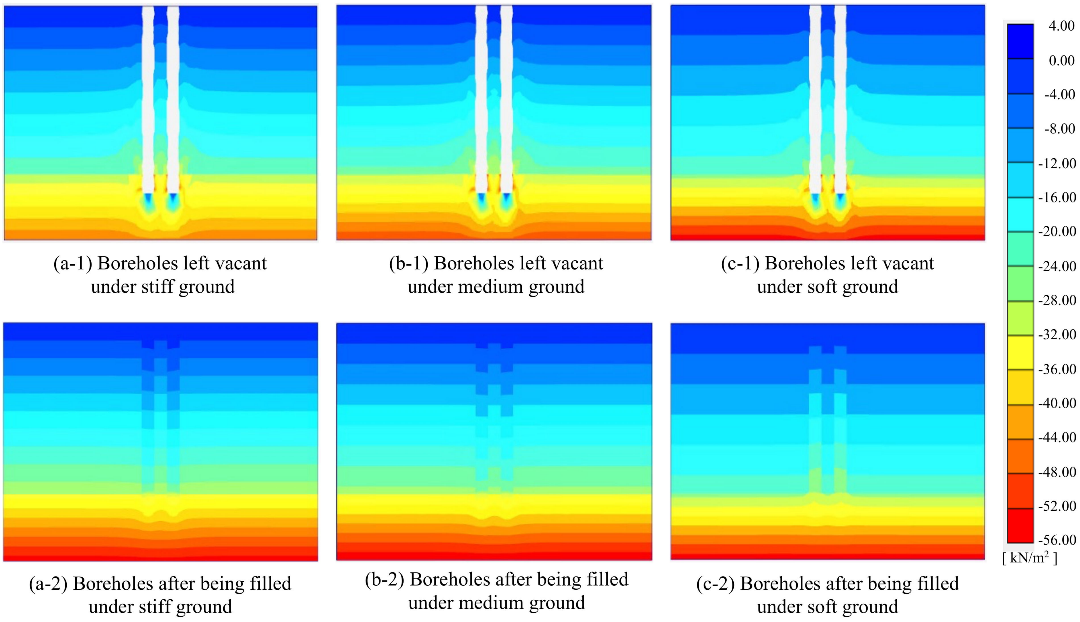

(a-1) Boreholes left vacant under stiff ground
(b-1) Boreholes left vacant under medium ground
(c-1) Boreholes left vacant under soft ground
(a-2) Boreholes after being filled under stiff ground
(b-2) Boreholes after being filled under medium ground
(c-2) Boreholes after being filled under soft ground

Figure 8. Comparison of frontal cross sectional total stress contour for vacant and filled cases of double boreholes.

Figure 9 shows a comparison of the amounts of total sinking of the different ground types for the vacant and filled double boreholes. Figure 10 shows a comparison of the pore water pressure of stiff, medium, and soft grounds in succession for the vacant and filled double boreholes. When the boreholes were filled with the filler material, stiff and medium grounds were seen to be uplifted by a small amount instead of experiencing settlement. The probable reason might be the upward stress caused by the action of filling the boreholes. As for soft ground, the amount of settlement was greatly reduced by the remaining concentrated stress. Overall, the settlement of the ground was largely avoided in the case of the filled boreholes. The pore water pressure recovered in all the ground types after the boreholes were filled. It was higher in stiff ground, with a recovery value of 0.06 kN/m^2, and it was same for medium and soft ground, with a recovery value of 0.04 kN/m^2.

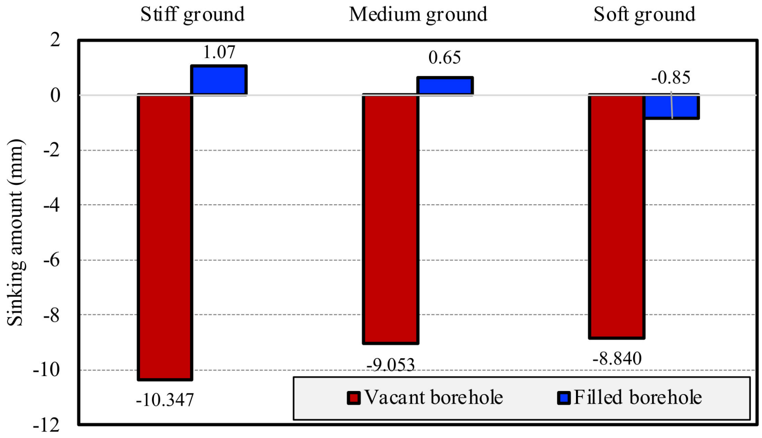

Figure 9. Comparison of sinking amounts for vacant and filled cases of double boreholes.

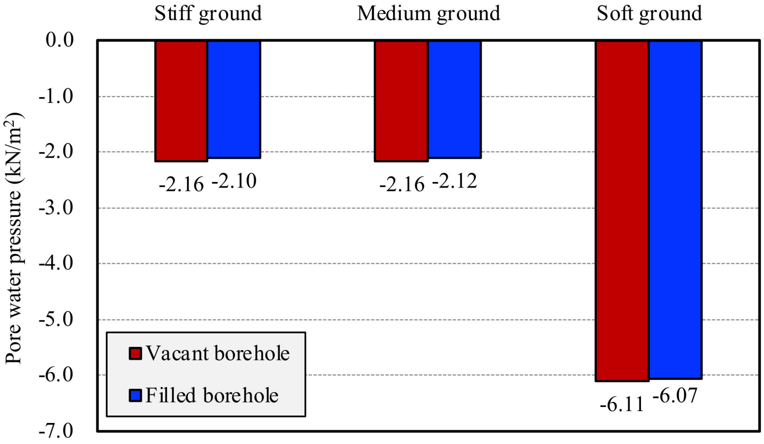

Figure 10. Comparison of porewater pressure for vacant and filled cases of double boreholes.

3.2. Influence of Loading on Ground Surrounding Boreholes

Figure 11 shows analytical models with loading for single and double boreholes at positions 1 and 2 in succession. Two steel paving plates, each 1.5 × 3.0 m in size and 22 mm thick, were placed over the area of 3 × 3 m, which acted as the dead load of 0.5 kN/m^2 magnitude. The load was set by considering that the load value would not become too large and affect the accuracy of the analysis results.

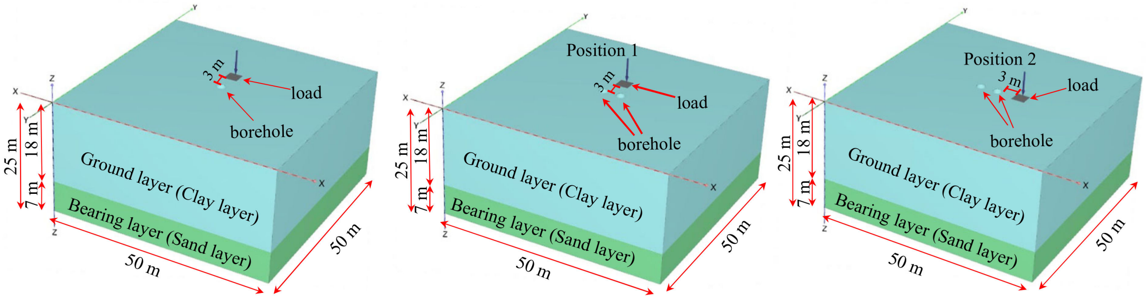

Figure 11. Analytical ground models for single and double boreholes under the loading condition.

3.2.1. In Case of Single Boreholes Left Vacant

Figure 12 shows the top views of the displacement contour for single boreholes with loading. Figure 13 shows a comparison of the rates of change in maximum displacement vectors for single boreholes with loading. The maximum displacement vectors for single boreholes without loading were observed at (25, 26, 0), (25, 26, 0), and (25.903, 25.429, −0.710) for stiff, medium, and soft grounds, respectively. When the load was applied, the maximum displacement vector coordinates shifted to (25, 26, 0), (25, 26, 0), and (25, 26, 0), respectively. The coordinates of the maximum displacement vectors remained unchanged for stiff and medium grounds, but they shifted toward the positive Y axis, in the direction of the loading location, for soft ground. This implies that only soft ground is likely to deform at different places depending upon the location of loading, which makes it more vulnerable than other ground types. The displacement and stabilization patterns were found to be the same as those of the unloaded case for all ground types. The displacement value increased by approximately 4 mm for the loading case in stiff and medium grounds, but it was only approximately 1 mm for soft ground. The overall deformation amount increased due to loading, and the value was higher for stiffer ground. Meanwhile, the deformation amount and the coordinates of the maximum deformation changed for soft ground, with the deformation inclining in the loading location.

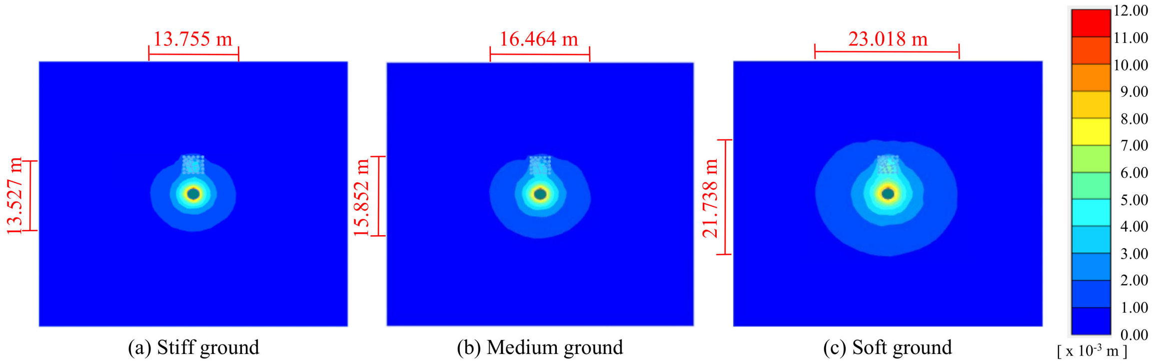

(a) Stiff ground (b) Medium ground (c) Soft ground

Figure 12. Top views of the displacement contour for single boreholes under the loading condition.

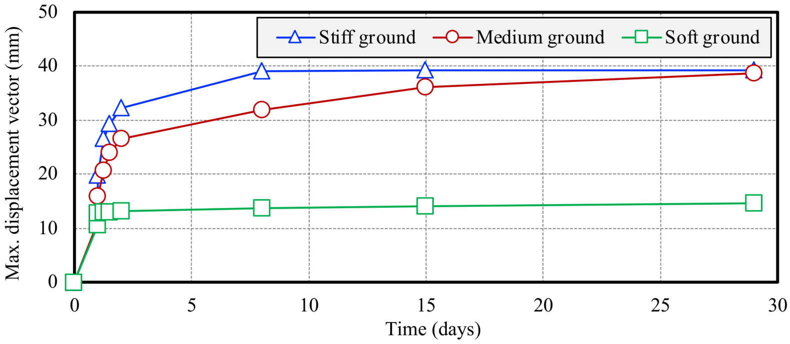

Figure 13. Rates of change in maximum displacement vectors for single boreholes under the loading condition.

3.2.2. In Case of Two Boreholes Left Vacant and Loading at Different Position

Figure 14 shows the top views of the displacement contour for the double borehole models, with loading at locations 1 and 2 in succession for grounds of different stiffness levels. Figure 15 shows a comparison of the rates of change in the maximum displacement vectors for double boreholes, with loading at position 1 or 2 in succession. The maximum displacement vectors for the double boreholes in a non-loaded condition were observed at the coordinates of (26.866, 25.5, 0), (26.866, 25.5, 0), and (23.966, 25.259, −0.428) for stiff, medium, and soft grounds, respectively. When loading was applied at position 1, the maximum displacement vector coordinates shifted to (23, 26, 0), (23, 26, 0), and (26.231, 25.639, −0.356), respectively, leaning toward the positive Y-axis. Additionally, when the loading was applied at position 2, the maximum displacement vector coordinates shifted to (26.134, 24.5, 0), (26.134, 24.5, 0), and (26.034, 24.741, −0.428), respectively, leaning toward the positive X axis. Thus, it can be concluded that the maximum displacement tends to occur in the direction of the load application.

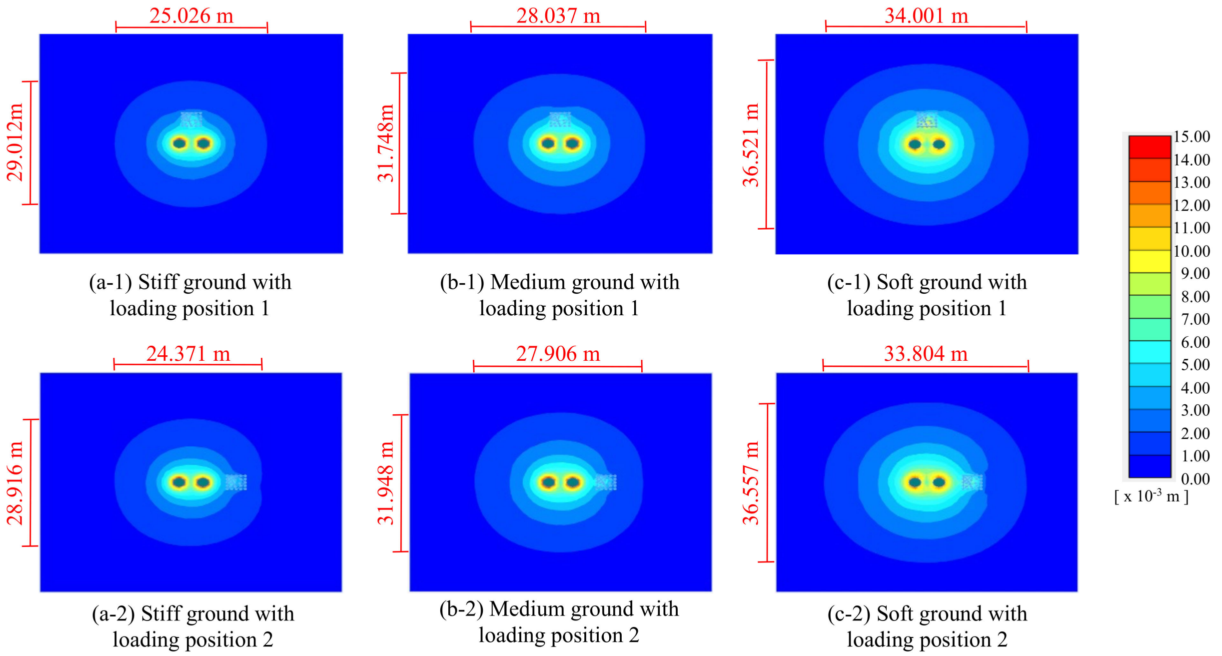

(a-1) Stiff ground with loading position 1

(b-1) Medium ground with loading position 1

(c-1) Soft ground with loading position 1

(a-2) Stiff ground with loading position 2

(b-2) Medium ground with loading position 2

(c-2) Soft ground with loading position 2

Figure 14. Top views of displacement contour for double boreholes under the loading condition.

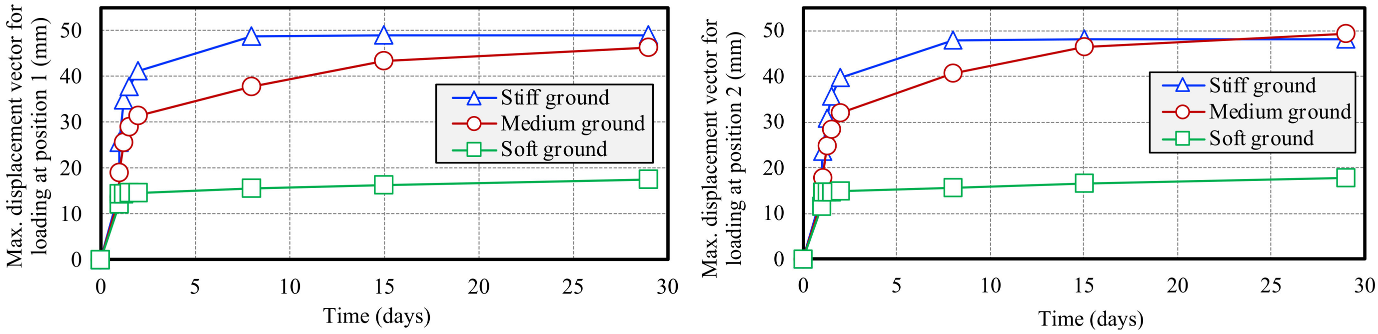

(**a**) Ground with loading position 1

(**b**) Ground with loading position 2

Figure 15. Rates of change in maximum displacement vectors for double boreholes under the loading condition.

However, there were no distinct changes in the intensity of the maximum displacement vector for either non-loading or loading at the different locations. The probable reason for this might lie in the assumption made during the simulation to reduce the calculation load.

Firstly, the load was not heavy enough to cause the maximum impact on the surrounding ground, as it was only 0.5 kN/m^2 spanning over 3 × 3 m. Next, the ground model contained only two boreholes; considering that the model is 50 × 50 m, the number of boreholes was too low to impart the maximum impact. For stiff ground, the maximum displacement vector value increased by approximately 2 mm in the case of loading at either position. For soft ground, the changes were negligible in both cases. Meanwhile, for medium ground, the value decreased by approximately 3 mm in the case of loading at position 1, but it remained unchanged in the case of loading at position 2. Although the overall influence of loading at either position remained negligible, the displacement of the ground between the load and the borehole increased, and the range of influence shifted toward the direction of the loading.

4. Conclusions

In this study, single and double boreholes were studied for cases with and without loading. The main focus was placed on the amount of maximum displacement experienced in each case. Additionally, a comparison was made for double boreholes in the cases of the boreholes being left vacant and being filled with filler material, and the parameters, such as the sinking amount and pore water pressure, were examined. From this study, the following conclusions can be drawn.

(1) The amount of ground displacement was seen to depend upon the stiffness of the ground. The maximum initial displacement was observed for stiff ground in all cases, except the case of double boreholes, in which the final stabilized displacement value was slightly higher or equal to that of the stiff ground.
(2) Soft ground was found to be relatively more unstable than stiff and medium grounds, as the location of the maximum deformation of this ground was different than that of the other grounds.
(3) The increase in the amount of displacement was observed to be larger for the case of an increased number of boreholes than that due to the loading.
(4) The surrounding ground remained settled if the boreholes were left vacant, but this settlement was prevented if the holes were immediately filled with appropriate filling material. Moreover, the pore water pressure recovery was higher for the filled condition.
(5) The presence of external loading not only contributed to an increase in the amount of displacement, but it also affected the location of the maximum displacement. It was observed that the inclination tended to occur in the direction of loading, indicating susceptibility to external loading.
(6) The influence on the horizontal range and maximum displacement vector of the surrounding ground was lower in location 2. In other words, borehole-related work conducted with machinery located in the existing pile alignment resulted in less influence on the ground.

This study was conducted for a maximum of two boreholes and was focused only on the deformation behavior. It did not consider the effect on the borehole wall during the progress of the pile removal. Future research should focus on improving the practicality of the conclusions by developing models based on the actual conditions of the site.

Author Contributions: Conceptualization, S.I. and S.K.; methodology, S.I. and K.N.; software, S.I.; validation, S.S., K.N. and S.I.; formal analysis, S.S.; investigation, S.K. and K.N.; resources, S.I.; data curation, S.S. and K.N.; writing—original draft preparation, S.S.; writing—review and editing, S.I.; visualization, S.I.; supervision, S.I.; project administration, S.I.; funding acquisition, S.I. and S.K. All authors have read and agreed to the published version of the manuscript.

Funding: This research received no external funding.

Institutional Review Board Statement: Not applicable.

Informed Consent Statement: Not applicable.

Data Availability Statement: Not applicable.

Conflicts of Interest: The authors declare no conflict of interest.

References

1. Yoshioka, S.; Kawasaki, H. Japan's high-growth postwar period (the role of economic plans). *ESRI Res. Note* **2016**, *27*, 1–82.
2. Inazumi, S.; Tanaka, S.; Komaki, T.; Kuwahara, S. Effect of insertion of casing by rotation on existing piles in removal of existing pile. *Geotech. Res.* **2021**, *8*, 25–37. [CrossRef]
3. Ministry of Land, Infrastructure, Transport and Tourism (MLIT). *Public Building Construction Standard Specification (Building Work)*, 2013th ed.; Ministry of Land, Infrastructure, Transport and Tourism: Tokyo, Japan, 2016.
4. Inazumi, S.; Kuwahara, S.; Jotisankasa, A.; Chaiprakaikeow, S. Construction method for pulling out existing piles and influence of pulling-out holes on the surrounding ground. *Geotech. Geol. Eng.* **2020**, *38*, 6107–6123. [CrossRef]
5. Kuwahara, S.; Inazumi, S.; Jotisankasa, A.; Chaiprakaikeow, S. Influence of the condition of pullout holes on the surrounding ground. *Int. J. Geo Eng.* **2020**, *11*, 10. [CrossRef]
6. Inazumi, S.; Hashimoto, R.; Shinsaka, T.; Nontananandh, S.; Chaiprakaikeow, S. Applicability of additives for ground improvement utilizing fine powder of waste glass. *Materials* **2021**, *14*, 5169. [CrossRef] [PubMed]
7. Inazumi, S.; Kuwahara, S.; Jotisankasa, A.; Chaiprakaikeow, S. Improvement mechanism of sodium carbonate on traditional composite filler. *Ground Improv.* **2021**, *174*, 132–139. [CrossRef]
8. Inazumi, S.; Namikawa, T.; Kuwahara, S.; Hamaguchi, S. Influence of pulling out existing piles on the surrounding ground. *Int. J. GEOMATE Geotech. Constr. Mater. Environ.* **2017**, *13*, 16–21. [CrossRef]
9. Inazumi, S.; Kuwahara, S.; Jotisankasa, A.; Chaiprakaikeow, S. MPS-CAE simulation on dynamic interaction between steel casing and existing pile when pulling out existing piles. *Int. J. Geomate Geotech. Constr. Mater. Environ.* **2020**, *18*, 68–73. [CrossRef]
10. Inazumi, S.; Kuwahara, S.; Nontananandh, S.; Jotisankasa, A.; Chaiprakaikeow, S. Numerical analysis for ground subsidence caused by extraction holes of removed piles. *Appl. Sci.* **2022**, *12*, 5481. [CrossRef]
11. Kawahara, T.; Kuwahara, S.; Inazumi, S.; Eguchi, T. Evaluation of the influence of filling material of existing pile extraction holes on the surrounding ground. In Proceedings of the JSCE 73rd Annual Conference, Sapporo, Japan, 29–30 August 2018; pp. 255–256.
12. Nontananandh, S.; Kuwahara, S.; Shishido, K.; Inazumi, S. Influence of perforated soils on installation of new piles. *Appl. Sci.* **2022**, *12*, 7712. [CrossRef]
13. Inazumi, S.; Kaneko, M.; Tomoda, Y.; Shigematsu, Y.; Shishido, K. Evaluation of flow-ability on fluidization treated soils based on flow analysis by MPS method. *Int. J. GEOMATE Geotech. Constr. Mater. Environ.* **2017**, *12*, 53–58. [CrossRef]
14. Inazumi, S.; Kaneko, M.; Shigematsu, Y.; Shishido, K. Fluidity evaluation of fluidisation treated soils based on the moving particle semi-implicit method. *Int. J. Geotech. Eng.* **2018**, *12*, 325–336. [CrossRef]
15. Inazumi, S.; Shigematsu, Y.; Nakao, K.; Shishido, K. 3-D particle flow analysis for fluidization treated soils. *Am. J. Civ. Environ. Eng.* **2018**, *3*, 59–67.
16. Wheeler, S.J.; Sharma, R.J.; Buisson, M.S.R. Coupling of hydraulic hysteresis and stress-strain behaviour in unsaturated soils. *Geotechnique* **2003**, *53*, 41–54. [CrossRef]
17. Wheeler, S.J. Inclusion of specific water volume within an elasto-plastic model for unsaturated soil. *Can. Geotech. J.* **1996**, *33*, 42–57. [CrossRef]
18. Alonso, E.E.; Gens, A.; Hight, D.W. Special Problem Soils. In Proceedings of the 9th European Conference on Soil Mechanics and Foundation Engineering, Dublin, Ireland, 31 August–3 September 1987; Volume 3, pp. 1087–1146.
19. Fredlund, D.G.; Morgenstern, N.R. Stress state variables for unsaturated soils. *J. Geotech. Eng. Div.* **1977**, *103*, 447–466. [CrossRef]
20. Fredlund, D.G.; Morgenstern, N.R.; Widger, R.A. The shear strength of unsaturated soils. *Can. Geotech. J.* **1978**, *15*, 313–321. [CrossRef]
21. Pradhan, K.K.; Chakraverty, S. Chapter Four-Finite Element Method. *Comput. Struct. Mech. Stat. Dyn. Behav.* **2019**, 25–28. [CrossRef]
22. Okamoto, K. Chapter 6—Finite Element Method. In *Fundamentals of Optical Waveguides*, 3rd ed.; Academic Press: Cambridge, MA, USA, 2022; pp. 271–338. [CrossRef]
23. Ramirez, W.F. Chapter 8—Solution of Partial Differential Equations. In *Computational Methods in Process Simulation*, 2nd ed.; Elsevier: Amsterdam, The Netherlands, 1997; pp. 353–430. [CrossRef]
24. Rapp, B.E. Finite Element Method. In *Microfluidics: Modelling, Mechanics and Mathematics*; Elsevier: Amsterdam, The Netherlands, 2017.
25. Ghasemzadeh, H.; Soujoudi, M.H.; Ghoreishian Amiri, S.A.; Karami, M.H. Elastoplastic model for hydro-mechanical behaviour of unsaturated soils. *Soils Found.* **2017**, *57*, 371–383. [CrossRef]
26. Roscoe, K.H.; Burland, J.B. *On the Generalised Stress-Strain Behaviour of Wet Clay*; Cambridge University Press: Cambridge, UK, 1968; pp. 535–609.
27. Liu, K.; Chen, S.L.; Voyiadjis, G.Z. Integration of anisotropic modified Cam Clay model in finite element analysis: Formulation, validation, and application. *Comput. Geotech.* **2019**, *116*, 103198. [CrossRef]

28. Borja, R.I. Cam-Clay plasticity, Part II: Implicit integration of constitutive equation based on a nonlinear elastic stress predictor. *Comput. Methods Appl. Mech. Eng.* **1991**, *88*, 225–240. [CrossRef]
29. Borja, R.I.; Lee, S.R. Cam-clay plasticity, Part 1: Implicit integration of elasto-plastic constitutive relations. *Comput. Methods Appl. Mech. Eng.* **1990**, *78*, 49–72. [CrossRef]
30. Perić, D. Analytical solutions for a three-invariant Cam clay model subjected to drained loading histories. *Int. J. Numer. Anal. Methods Geomech.* **2006**, *30*, 363–387. [CrossRef]
31. Xu, S.; Xu, G.; Cheng, Y. Review of Cam-Clay model development of soil. *Acad. J. Yangtze River Acad. Sci. People's Repub. China* **2007**, *24*, 3.
32. Ikegami, S.; Mizuno, K.; Kiyama, N.; Kinoshita, H.; Tsuchida, T. Evaluation and case analysis of lateral deformation prediction of soft ground. *Geotech. Eng. Constr.* **2007**, *25*, 133–144.
33. Murakami, T.; Niihara, Y.; Yamada, T.; Ohno, S.; Noguchi, T.; Miyata, M. Deformation prediction of large-scale seawall structures by elasto-viscoplastic FEM analysis. *J. Jpn. Soc. Civil. Eng. C* **2012**, *68*, 224–238.
34. Kawamura, S.; Ekisaka, K.; Aso, K. Consideration on soil characteristic values in ground in Yamaguchi prefecture. *J. Chugoku Branch Jpn. Geotech. Soc. Soils Constr.* **2017**, *35*, 185–190.
35. Japan Road Association. *Road Earthworks-Embankment Guidelines*, 14th ed.; Japan Road Association: Tokyo, Japan, 2022; p. 101.